ValerieX (VXXX)

Volume III — Computational Layer

C-Family Predictions, Figures, Capsule Discriminator, and the Transient-Drag Bridge

Nicholas Parkyn

Independent Researcher · nikparkyn@googlemail.com

Supporting deep-dive to the main manuscript

Set V2.0 · May 2026

Abstract

Volume III is the computational deep-dive companion to the main ValerieX manuscript. It translates the geometry-aware general law $a = g(\rho_o - \rho_m)/(\rho_o + C\rho_m)$ into rendered figures, numerical predictions, and computational anchors. Five figures are produced: the master family curve (Fig. 1); the intermediate-density discriminator at $r = 2$ (Fig. 2); the continuous C-spectrum (Fig. 3); the capsule continuous-geometry curve $C(L/D)$ derived from prolate-spheroid added-mass theory (Fig. 4); and the difference plot identifying the optimal discrimination region (Fig. 5).

The capsule prediction sharpens the framework's most discriminating experiment from a binary sphere-vs-cylinder comparison into a continuous-parameter falsification test. The McKee & Czarnecki (2019) sphere-branch result is shown to be the published numerical anchor for the $C = 0.5$ branch. A worked transient-drag integration links the early-time C-family acceleration to drag-limited terminal motion through a classical-compatible closure that adds no new free parameters beyond geometry-set C and standard drag descriptors.

Keywords: ValerieX, C-family, Atwood number, added-mass coefficient, participating medium load, capsule discriminator, prolate-spheroid theory, transient drag integration, McKee & Czarnecki anchor.

1 Role of this Volume

Where Volume I establishes *what the law is* and Volume II establishes *how motion is expressed across regimes*, Volume III establishes *what numerical predictions follow* and provides the figures and computational anchors that support the experimental programme of Volume IV.

The deliverables of this volume are concrete:

- Five rendered figures with their underlying numerical tables (§§3–6, 8).
- A quantitative $C(L/D)$ prediction for capsule bodies derived from classical added-mass theory (§6).
- A numerical anchor against the McKee & Czarnecki (2019) sphere-branch data (§7).
- A reference one-function implementation of the C-family law (§9).

- A worked transient-drag integration that connects early-time C-family predictions to terminal motion (§9.3).

2 Mathematical Framework

2.1 Governing Equation

The general form $a = g(\rho_o - \rho_m)/(\rho_o + C\rho_m)$ represents a one-parameter family of acceleration laws indexed by the participation coefficient C. Members of this family are unified by their dependence on the density contrast $(\rho_o - \rho_m)$ and differ only in how the surrounding medium contributes to the effective inertia of the system.

2.2 Normalised Form

Define the density ratio $r = \rho_o/\rho_m$. The governing law becomes

$$\frac{a}{g} = \frac{r-1}{r+C}.$$

This removes dimensional dependence on the absolute density scale, allowing direct comparison across systems with different ρ_m and direct experimental scaling between water-based and other-medium configurations. The bounded contrast $\chi = (\rho_o - \rho_m)/(\rho_o + \rho_m)$ is mathematically identical to the classical Atwood number, recovered as the $C = 1$ branch.

2.3 Key Properties

- *Equilibrium:* $r = 1 \Rightarrow a = 0$.
- *Saturation:* as $r \to \infty$, $a \to g$ for every C.
- *Vacuum recovery:* as $\rho_m \to 0$ all C-branches collapse to $a = g$, recovering the Apollo 15 / Galileo equivalence.
- *Label-exchange algebraic property:* antisymmetry under $\rho_o \leftrightarrow \rho_m$ holds only at $C = 1$.
- *Boundedness:* $|a/g| < 1$ across the full range of finite r holds only at $C = 1$; every other branch diverges below the $-g$ bound for sufficiently small r.

The vacuum limit is therefore not a discriminator between members of the C-family. Vacuum free-fall comparisons serve as positive controls for the apparatus and the saturation limit, but cannot distinguish between competing predictions: the discrimination is intrinsically a finite-medium measurement at intermediate density and shape-controlled coupling.

3 C-Family Overview (Figure 1)

3.1 Reference Branches

Three members of the C-family are sufficient to define the primary discriminator structure.

Model	C	Acceleration expression
Classical (object-normalised)	0	$a = g(r-1)/r$

Model	C	Acceleration expression
Sphere (potential flow)	0.5	$a = g(r-1)/(r+0.5)$
ValerieX (cylinder $\perp$ axis)	1	$a = g(r-1)/(r+1)$

3.2 Behavioural Differences

- All three branches converge at vacuum saturation ($r \gg 1$): $a/g \to 1$.
- All three branches meet exactly at equilibrium ($r = 1$): $a/g = 0$.
- The branches diverge progressively as r decreases below unity, with maximum divergence in the buoyant regime ($r < 1$) for the $C = 0$ branch and at the intermediate-density falling regime ($1 < r \lesssim 5$) for the experimentally clean test point.

Figure 1 — C-family acceleration curves

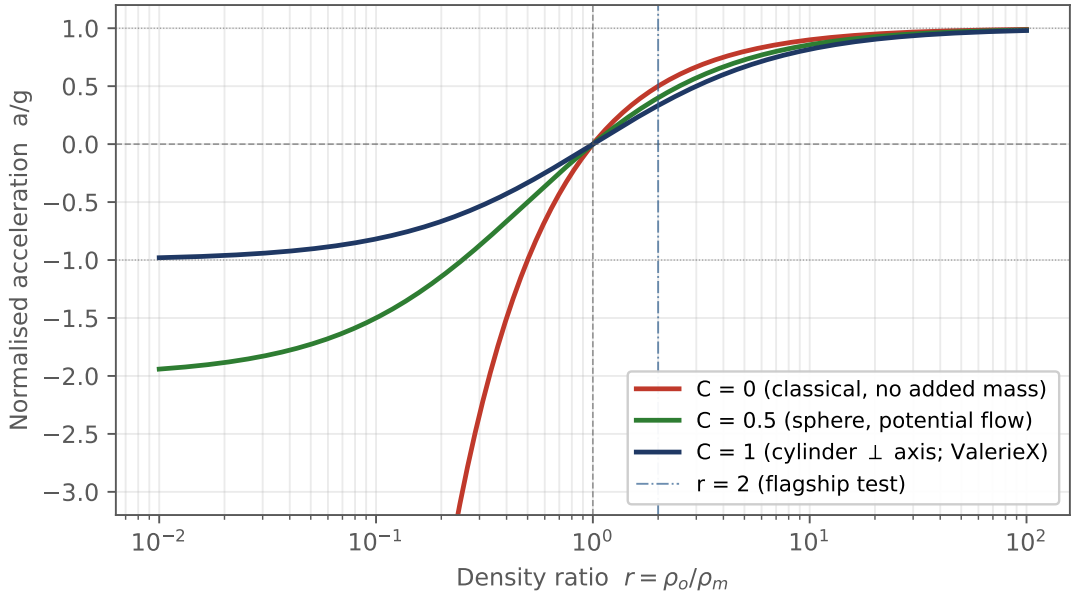

Figure 1. Normalised initial acceleration a/g as a function of the density ratio $r = \rho_\mathrm{o}/\rho_\mathrm{m}$ on a logarithmic axis, for three participation coefficients: $C = 0$ (classical, no added-mass; red), $C = 0.5$ (rigid sphere in inviscid potential flow; green), $C = 1$ (cylinder $\perp$ axis; ValerieX bounded form; navy). Vertical dashed line marks equilibrium $r = 1$; the dot-dash line marks the flagship test point $r = 2$. The $C = 1$ branch remains bounded $|a/g| < 1$ across the full range of finite r, while the $C = 0$ branch diverges below the $-g$ floor as $r \to 0$.

4 Intermediate-Density Discriminator (Figure 2)

4.1 The $r = 2$ Test Point

At $\rho_\mathrm{o} = 2\rho_\mathrm{m}$, the C-family predictions separate by experimentally accessible margins.

Branch	C	a/g	$a\ (\mathrm{m\,s^{-2}})$
Classical (no added-mass)	0	0.5000	4.903

Branch	C	a/g	$a\,(\mathrm{m\,s^{-2}})$
Sphere (potential flow)	0.5	0.4000	3.923
ValerieX (cylinder $\perp$ axis)	1	0.3333	3.269

4.2 Discrimination Margins

- $C = 0$ *vs* $C = 1$*:* 0.1667 $g \approx 1.634\,\mathrm{m\,s^{-2}}$ ($\sim 33\%$ of g). Resolvable on commodity high-speed video at ≥ 240 fps.
- $C = 0.5$ *vs* $C = 1$*:* 0.0667 $g \approx 0.654\,\mathrm{m\,s^{-2}}$ ($\sim 6.7\%$ of g). Requires ≥ 1000 fps imaging and sub-millimetre tracking. At $t = 30$ ms after release this corresponds to a position difference of ~ 0.3 mm.
- $C = 0$ *vs* $C = 0.5$*:* 0.1000 $g \approx 0.981\,\mathrm{m\,s^{-2}}$. Resolvable on commodity equipment.

5 Continuous C-Spectrum (Figure 3)

5.1 Physical Meaning of C

Within ValerieX, C represents the degree to which the surrounding medium participates in motion when density-state disequilibrium resolves. It is the dimensionless coefficient that scales the participating-medium load $(\rho_\mathrm{o} + C\rho_\mathrm{m})V$ relative to the object load $\rho_\mathrm{o}V$. Geometry, orientation, and surface interaction together set how much of the medium is co-disturbed.

In the broader drive–coupling–resistance separation: density-state contrast $(\rho_\mathrm{o} - \rho_\mathrm{m})$ is the drive; C is the coupling term; viscosity is the resistance term. C is not a universal constant: it is a measurable coupling parameter that varies with shape and orientation.

5.2 Continuous Spectrum

A central extension introduced in this volume is to treat C as a continuous parameter rather than a small set of discrete tabulated cases. The full continuous range $0 \leq C \leq 1$ admits intermediate values for any geometry that lies between the sphere (minimal participation) and the perpendicular cylinder (maximal participation). The capsule discriminator of §6 makes this prediction quantitative.

6 Capsule Discriminator (Figure 4)

6.1 Why This Geometry Matters

The capsule — a circular cylinder closed at each end by a hemisphere of equal radius — is the geometry that interpolates most directly between the two reference cases of the C-family. It approaches the sphere in the limit of zero cylindrical length (the two hemispheres meet to form a full sphere, $C \to 0.5$) and approaches the perpendicular cylinder in the limit of long aspect ratio ($C \to 1$). By varying the cylindrical-section length while holding the cross-sectional radius fixed, the capsule sweeps out a continuous range of effective participation coefficients while keeping the density ratio invariant.

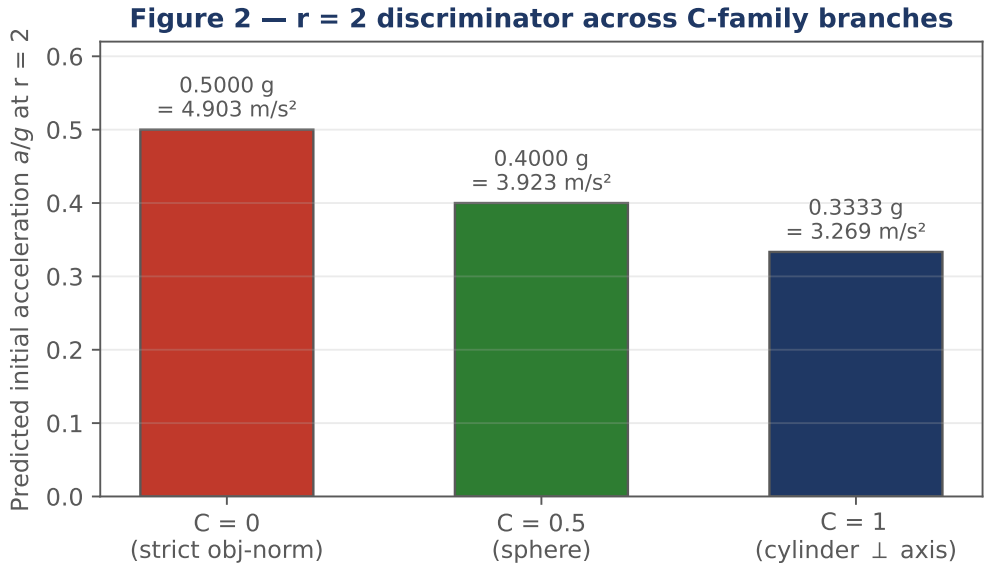

Figure 2. Predicted initial acceleration at $r = 2$ across the three reference branches. The $C = 0$ vs $C = 1$ separation ($\sim 33\%$ of g) is the flagship discriminator and is resolvable on commodity equipment; the $C = 0.5$ vs $C = 1$ separation ($\sim 7\%$ of g) is the sphere-vs-cylinder discriminator and requires higher-frame-rate imaging.

6.2 Predicted $C(L/D)$ from Prolate-Spheroid Theory

The capsule participation coefficient is computed as a function of cylindrical-section aspect ratio L/D using the closed-form added-mass coefficient for a prolate spheroid in motion perpendicular to its long axis (Lamb 1932 §126; Brennen 1982 Table 1). For a prolate spheroid with semi-major axis a and semi-minor axis b, motion perpendicular to the long axis gives an added-mass coefficient

$$k_{\perp} = \frac{\beta_0}{2 - \beta_0},$$

where $\beta_0 = 1/e^2 - [(1 - e^2)/(2e^3)] \cdot \ln[(1 + e)/(1 - e)]$ and $e = \sqrt{1 - (b/a)^2}$ is the spheroid eccentricity.

For a capsule of cylindrical-section length L and end-cap diameter D, the body is mapped to an equivalent prolate spheroid of aspect ratio $a/b = (L/D) + 1$. This matches both limits exactly: at $L/D = 0$ the capsule is a sphere ($a/b = 1$, $k_{\perp} = 0.5$); as $L/D \to \infty$ the capsule approaches an infinite cylinder ($a/b \to \infty$, $k_{\perp} \to 1$). Set $C = k_{\perp}$.

L/D	Spheroid a/b	Predicted C	a/g at r = 2	a at r = 2 ($\mathrm{m\,s^{-2}}$)
0.0	1.00	0.500	0.4000	3.923
0.5	1.50	0.580	0.3949	3.872
1.0	2.00	0.704	0.3698	3.626
1.5	2.50	0.781	0.3601	3.531
2.0	3.00	0.804	0.3566	3.498
3.0	4.00	0.864	0.3494	3.426
4.0	5.00	0.890	0.3461	3.394

L/D	Spheroid a/b	Predicted C	a/g at r = 2	a at r = 2 ($\mathrm{m\,s^{-2}}$)
6.0	7.00	0.929	0.3414	3.348
8.0	9.00	0.954	0.3386	3.320

The mapping $a/b = L/D+1$ is a first-order approximation. Capsules differ from prolate spheroids by their hemispherical end-caps; CFD or boundary-element calculation can produce a more accurate curve if needed. The ordering predicted here — $a_{\text{sphere}}(r) > a_{\text{capsule}}(r) > a_{\text{cylinder}}(r)$ at fixed $r > 1$, monotonic in L/D — is the structural prediction of the framework and does not depend sensitively on the spheroid mapping.

7 Sphere Branch Numerical Anchor (McKee & Czarnecki 2019)

McKee & Czarnecki (2019) report buoyant-rise initial-acceleration measurements for light spheres in water, and find that the observed accelerations are reproduced only when the participating-medium-load renormalisation $(\rho_{\mathrm{o}} + 0.5\rho_{\mathrm{m}})V$ is applied to the effective inertia. This is exactly the $C = 0.5$ sphere branch of the C-family. Their measurement therefore stands as a positive published anchor for one specific branch of the framework.

The table below tabulates the $C = 0.5$ prediction across the buoyant-rise density-ratio range probed by their work, alongside the $C = 0$ strict object-normalised limit (which their data already rules out) and the $C = 1$ cylinder $\perp$-axis branch (against which they do not test).

$r = \rho_{\mathrm{o}}/\rho_{\mathrm{m}}$	χ	a/g $(C = 0.5)$	a ($\mathrm{m\,s^{-2}}$)	a/g $(C = 0)$	a/g $(C = 1)$
0.10	-0.818	-1.500	-14.71	-9.000	-0.818
0.25	-0.600	-1.000	-9.807	-3.000	-0.600
0.40	-0.429	-0.667	-6.538	-1.500	-0.429
0.60	-0.250	-0.364	-3.566	-0.667	-0.250
0.80	-0.111	-0.154	-1.509	-0.250	-0.111

The $C = 0$ column produces $|a/g| > 1$ throughout the buoyant-rise regime ($r < 1$), which contradicts observation: bounded buoyant rise does not exceed g in magnitude. McKee & Czarnecki's data require the sphere branch $C = 0.5$ specifically. The experimental gap that Volume IV is designed to fill is the equivalent published anchor for the cylinder $\perp$-axis ($C = 1$) branch and for the continuous-parameter capsule curve of §6.

8 Reference Implementation

8.1 Core C-Family Function

The full predictive content of the early-time C-family is captured by a single function. The implementation below is the same one used to generate Figures 1–5 and the tables above.

```
def acceleration(r, C, g=9.80665):
    """ValerieX C-family acceleration in a participating medium.
```

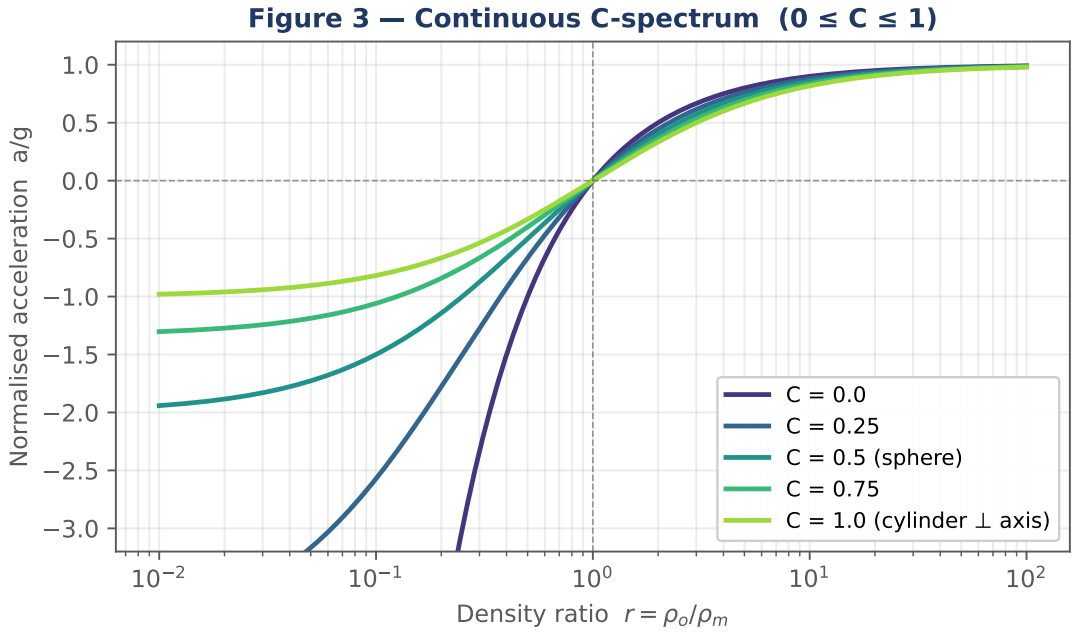

Figure 3. C-family acceleration curves for representative values $C \in \{0, 0.25, 0.5, 0.75, 1.0\}$ on the same logarithmic density-ratio axis as Figure 1. Capsule geometries are predicted to interpolate continuously between the sphere ($C = 0.5$) and cylinder ($C = 1$) curves; the L/D dependence is computed in §6.

```
    r :  array_like - density ratio rho_o / rho_m (dimensionless)
    C : float - participation coefficient (0 <= C <= 1)
    g :  float - local environmental ceiling (m s^-2; NIST CODATA)
    Returns acceleration in m s^-2; sign carries direction.
    """
    return g * (r - 1.0) / (r + C)
```

8.2 Capsule $C(L/D)$ Reference Implementation

```
import numpy as np
def C_capsule_from_LD(LD):
    """Predicted participation coefficient for a hemisphere-ended capsule.
    LD : cylindrical-section aspect ratio L/D (≥ 0).
    Returns C in [0.5, 1.0).
    Maps capsule ->equivalent prolate spheroid of aspect ratio a/b = LD + 1,
    then evaluates Lamb (1932) §126 perpendicular added-mass coefficient.
    """
    aspect = LD + 1.0
    if aspect <= 1.0:  return 0.5
    e = np.sqrt(1.0 - 1.0 / aspect**2)
    beta0 = 1.0/e**2 - (1.0 - e**2)/(2.0*e**3) * np.log((1.0+e)/(1.0-e))
    return beta0 / (2.0 - beta0)
```

8.3 Transient Drag Integration

The early-time C-family acceleration is the $t \to 0^+$ limit of the full transient motion. For times after release, drag closure becomes important. The effective participating inertia is $m_{\text{eff}} =$

Figure 4 — Predicted capsule C(L/D) from prolate-spheroid added-mass th

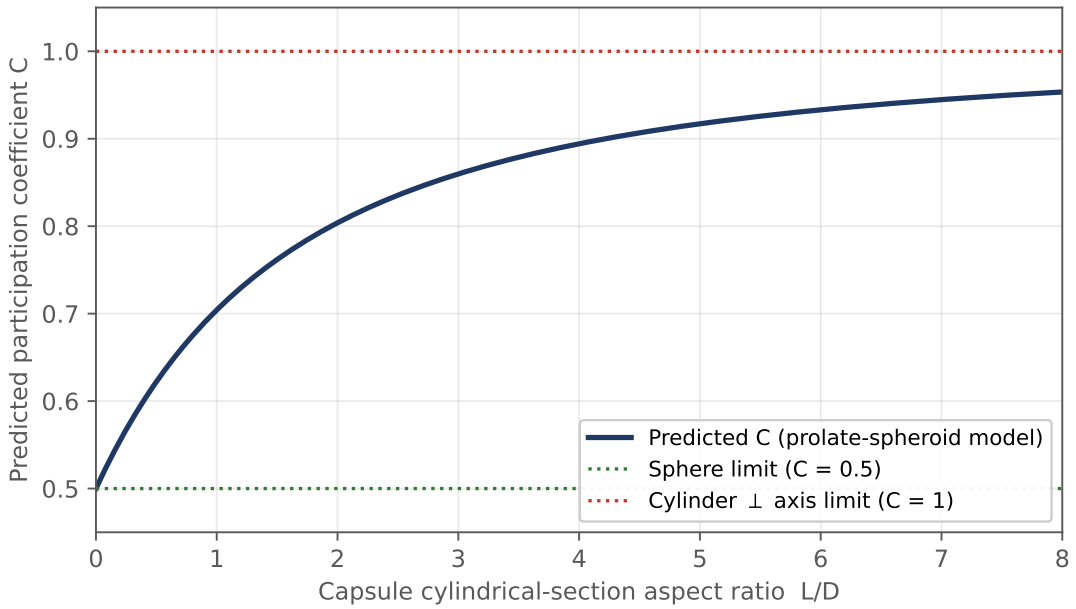

Figure 4. Predicted capsule participation coefficient C as a function of cylindrical-section aspect ratio L/D, computed from prolate-spheroid added-mass theory for motion perpendicular to the long axis. The curve passes exactly through the sphere limit $C = 0.5$ at $L/D = 0$ and approaches the cylinder $\perp$-axis limit $C = 1$ monotonically. This curve converts the capsule shape-controlled experiment from a binary discriminator into a continuous-parameter falsification test: any monotonic L/D trend in measured early-time acceleration that does not track this curve would directly challenge the prolate-spheroid mapping or the C-family structure.

$(\rho_o + C\rho_m)V$; the drive term is $F_{\text{drive}} = (\rho_o - \rho_m)Vg$; the resistance term combines Stokes-linear and bluff-body quadratic drag:

$$D(v) \;=\; 6\pi\eta R v + \tfrac{1}{2}\rho_m C_d A|v|v.$$

The full transient ODE is $dv/dt \;=\; [F_{\text{drive}} - D(v)]/m_{\text{eff}}$. At $v = 0$ the drag term vanishes identically and dv/dt reduces to the early-time C-family acceleration — the integration is therefore continuous with the early-time predictions used by the experimental programme.

```
from scipy.integrate import solve_ivp
import numpy as np
def simulate(rho_o, rho_m, V, C, mu, R, A, Cd,
        g=9.80665, t_max=2.0, n_pts=2000):
    """Full transient ODE: drive - drag, with C-family inertia."""
    m_eff = (rho_o + C * rho_m) * V
    F_drive = (rho_o - rho_m) * V * g
    def rhs(t, y):
        z, v = y
        D = 6 * np.pi * mu * R * v + 0.5 * rho_m * Cd * A * abs(v) * v
        return [v, (F_drive - D) / m_eff]
    sol = solve_ivp(rhs, [0, t_max], [0.0, 0.0],
        t_eval=np.linspace(0, t_max, n_pts), method="LSODA",
```

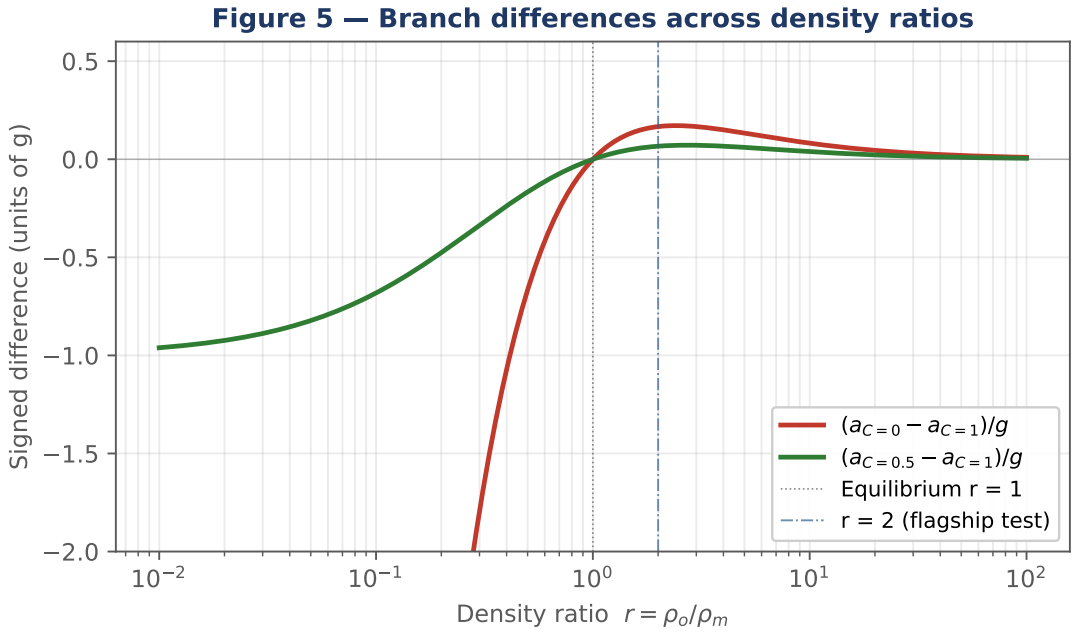

Figure 5. Signed differences $(a_{C=0} - a_{C=1})/g$ and $(a_{C=0.5} - a_{C=1})/g$ across density ratios. The differences vanish at equilibrium ($r = 1$) and at vacuum saturation ($r \to \infty$). The largest absolute deviation occurs in the deep-buoyant regime ($r \ll 1$), where the strict object-normalised $C = 0$ branch diverges below the $-g$ bound while the $C = 1$ branch remains bounded. The intermediate-falling regime ($1 < r \lesssim 5$) is the experimentally optimal discrimination region.

```
    rtol=1e-8, atol=1e-10)
return sol.t, sol.y[0], sol.y[1]
```

Self-consistency check. At $t = 0$, dv/dt evaluates to $g(r-1)/(r+C)$ within solver tolerance, recovering the early-time C-family acceleration of Volume I exactly. The transient model adds no new free parameters beyond C (set by geometry) and the standard drag descriptors μ, R, A, C_d drawn from classical fluid mechanics.

9 Limitations and Open Questions

The simulation framework presented here covers the early-time C-family law and a classical-compatible transient closure. It does not include:

- A full Cavendish torque model. The supported-regime regime-classification observation of Volume II is structural; no quantitative density-state alternative to the conventional precision-G interpretation is asserted.
- Electromagnetic coupling equations beyond the structural role of EM as the field within which differentiated substance and density-state are possible.
- CFD-grade capsule $C(L/D)$ predictions. The prolate-spheroid mapping is a first-order approximation; CFD or boundary-element computation handling the hemispherical end-caps explicitly would refine the curve, particularly at small L/D.
- Non-terrestrial environments. $g = 9.80665\,\mathrm{m\,s^{-2}}$ is treated as the locally observed environmen-

tal ceiling. Extensions to other ceilings would require independent measurement.

These are stated as boundaries of the present formulation rather than as defects.

10 Conclusion

Volume III completes the predictive layer of the ValerieX programme. It translates the bounded relational law of Volume I and the regime classification of Volume II into a quantitative, computational, and visual structure. The five figures define the falsification structure of the framework with the precision a reviewer or experimenter requires.

The capsule $C(L/D)$ prediction sharpens the framework's most discriminating experiment from a directional sphere-vs-cylinder comparison into a continuous-parameter falsification test. The McKee & Czarnecki (2019) sphere-branch anchor establishes that one specific branch of the C-family — $C = 0.5$ — already has positive published support. The transient-drag integration connects the early-time C-family predictions to drag-limited late-time motion through a classical-compatible closure that adds no new free parameters beyond geometry-set C and standard drag descriptors.

References (key)

Brennen, C. E. (1982). *A Review of Added Mass and Fluid Inertial Forces*. Naval CEL Report CR 82.010.
Galilei, G. (1638). *Discorsi*.
Gillies, G. T. (1997). The Newtonian gravitational constant. *Rep. Prog. Phys.* 60, 151–225.
Kelvin, Lord (W. Thomson) (1871). *Phil. Mag.* 42(281), 362–377.
Lamb, H. (1932). *Hydrodynamics*, 6th ed. Cambridge University Press.
McKee, K. & Czarnecki, A. (2019). *Am. J. Phys.* 87(3), 165–170.
NIST (2019). CODATA: $g_n = 9.80665\,\mathrm{m\,s^{-2}}$.
Reynolds, O. (1883). *Phil. Trans. Roy. Soc.* 174, 935–982.
Scott, D. (1971). *Apollo 15 Mission Report*. NASA MSC-05161.
Stokes, G. G. (1851). *Trans. Camb. Phil. Soc.* 9, 8–106.

End of Volume III — Set V2.0 — May 2026